Cement & Concrete Composites 34 (2012) 634–641

Contents lists available at SciVerse ScienceDirect

Cement & Concrete Composites

journal homepage: www.elsevier.com/locate/cemconcomp

Analysis of semi-adiabatic tests for the prediction of early-age behavior of massive concrete structures

Briffaut Matthieu [a,b,*], Benboudjema Farid [a], Torrenti Jean-Michel [c], Nahas Georges [a,b]

[a] LMT Cachan/ENS Cachan/CNRS UMR8535/UPMC/PRES UniverSud Paris, Cachan, France
[b] Institut de radioprotection et de sûreté nucléaire, Fontenay-aux-Roses, France
[c] Laboratoire Central des Ponts et Chaussées, Université Paris Est, Paris, France

ARTICLE INFO

Article history:
Received 3 June 2010
Received in revised form 31 August 2011
Accepted 1 September 2011
Available online 13 September 2011

Keywords:
Early-age
Temperature
Hydration
Concrete
Semi-adiabatic
Heat loss compensation

ABSTRACT

In this paper, experimental and numerical results on two types of semi-adiabatic tests have been compared. The semi-adiabatic tests are of particular interest since they are simple and easy to perform. However, their analysis may be still difficult since they are based on several assumptions that need to be addressed. In this paper, a numerical study has been undertaken for validating and rejecting some of these assumptions which may lead to misleading results. Moreover, the effect of apparent activation energy, which is a key role parameter for the prediction of hydration, has been studied. It shows that a dual study is required for both the identification and the prediction of early-age behavior of massive concrete structures.

1. Introduction

Prediction of hydration degree and temperature evolution is a major concern for massive concrete structures such as foundations, dams, nuclear containment structures, gas and water tanks, and tunnels. Indeed, temperature gradients may lead to early-age cracking and thus reduce the serviceability of these structures (due to faster migration of aggressive species, reduction of the tightness, etc.) This cracking is also strongly dependent upon the evolutions of Young modulus, tensile strength, creep strains, which are also affected by the evolution of hydration degree and temperature.

In order to identify the release of heat (and temperature field) or the evolution of hydration degree in concrete elements, semi-adiabatic tests are of particular interest, since they are simple and easy to perform. They require only the measure of temperatures, in comparison with adiabatic tests for instance, as described below (e.g. [1–4]). Indeed, in adiabatic tests, the curing chamber (or calorimeter), surrounding the concrete specimen, is kept at the same temperature as the concrete specimen to reduce heat losses. A perfect insulation is impossible to provide. Therefore, it requires a control system and an active circulation of a fluid (air or water) around the concrete specimen (e.g. [5–8]). An exhaustive review of semi-adiabatic and adiabatic testing has been made by Springenschmidt [9].

In semi-adiabatic tests, heat losses are strongly limited by a thermal insulation. They can be classified in two categories, depending on the type of insulation (insulation material or vacuum). Both types are studied in this paper:

- The Langavant insulated bottle (type of insulation: vacuum), which is a normalized device commonly used in France [10] and which has been recently normalized by the European community [11].
- A quasi-adiabatic test (type of insulation: insulating material), developed at the Laboratoire Central des Ponts et Chaussées (LCPC), commonly used in France in laboratory or in building sites [12] and which will be called QAB test. The principle of this test is to measure the temperature evolution of a concrete specimen (a cylinder with a 16 cm diameter and a 32 cm height) placed into an insulated box.

The interpretation of the results for both methods requires first the calibration of the device (heat capacity μ and heat loss α). Next, knowing the heat capacity of the concrete specimen (C_{con} [J °C^{-1}]), the temperature of the concrete specimen T_{con} and the exterior temperature T_{ext}, the release of hydration heat (q) reads:

* Corresponding author at: LMT Cachan/ENS Cachan/CNRS UMR8535/UPMC/PRES UniverSud Paris, Cachan, France. Tel.: +33 1 47 40 53 69; fax: +33 1 47 40 74 65.
E-mail address: briffaut@lmt.ens-cachan.fr (B. Matthieu).

0958-9465/$ - see front matter © 2012 Published by Elsevier Ltd.
doi:10.1016/j.cemconcomp.2011.09.001

$$q(t_{sa}) = C_{con}(T_{ad}(t_{sa}) - T_{ad}(t_{sa}=0)) = C_{tot}(T_{con}(t_{sa}) - T_{con}(t_{sa}=0)) + \int_0^{t_{sa}} (a + b\theta(t))\theta(t)dt \quad (1)$$

where C_{tot} [J °C^{-1}] is the total heat capacity (concrete + calorimeter), a [W] and b [W °C^{-1}] are coefficients of heat loss of the calorimeter (with $\alpha = a + b\theta$), t_{sa} [s] is the «real» time related to the semi-adiabatic test, $\theta = T_{con} - T_{ext}$ is the heating of the concrete specimen and T_{ad} is the theoretical adiabatic temperature. The right term of Eq. (1) corresponds to the compensation, deduced from the calibration of heat loss. It is usual to calculate the theoretical adiabatic temperature in order to identify the material parameters involved in the prediction of hydration degree and temperature profile in concrete structures (e.g. [13–16]).

Since the hydration is an exothermic reaction, time must be corrected and related to a reference temperature (20 °C or the theoretical adiabatic temperature T_{ad} for instance), like in the maturity concept (e.g. [15]). Thus, the release of heat during an adiabatic test will be faster (compared to a semi-adiabatic test) and the link between the time scale associated with the semi-adiabatic test t_{sa} and associated to the adiabatic test t_{ad} is obtained through the following relationship (supposing that the thermo-activation is governed by the Arrhenius law [17]):

$$t_{ad} = \int_0^{t_{sa}} e^{\frac{E_a}{R}\left[\frac{1}{(273+T_{ad}(t))} - \frac{1}{(273+T_{con}(t))}\right]} dt \quad (2)$$

where E_a is the apparent activation energy of cement [J mol^{-1}] and R is the constant of perfect gas [8.314 J mol^{-1} K^{-1}]

From these results, the release of hydration heat and the hydration degree can be predicted whatever is the history of temperature (e.g. [14]).

However, some shortcomings need to be addressed:

- The apparent activation energy has to be determined. This can be done approximately from the knowledge of some chemical characteristics of the cement [18] or from experiments (e.g. [19,18]). However, it depends upon temperature (several chemical reactions, with different kinetics and different values of apparent activation energy, occur during hydration of cement) and the type of experimental devices (e.g. Grube quoted in [9,20,21]). For the sake of simplicity, it is assumed here, as is done for most of the models (e.g. [14,22,23,16]), that this parameter is constant.
- The calibration of the semi-adiabatic devices is performed in steady state conditions, although the analysis of the results (Eq. (1)) is performed in transient conditions. The heat loss coefficient α is supposed to be linear with respect to the temperature difference between concrete and environment (hypothesis 1).
- The heat loss compensation is based on the assumption that the temperature in the calorimeter and the concrete specimen are equal and uniform (Eq. (1); hypothesis 2).

Therefore, a numerical analysis of these semi-adiabatic devices has been undertaken in order to check the ability of conventional models [13,14,23,16] to reproduce experimental results and also to justify the two aforementioned hypotheses. In addition, the location of the temperature sensor is discussed. Finally, a parametric study has been performed in order to emphasize the role played by the apparent activation energy in the process of identification of material parameters (for the prediction of temperature in a massive concrete structure).

2. QAB (semi-adiabatic) test

2.1. Mesh and model

2.1.1. Mesh

In the QAB test, the concrete specimen is cylindrical and the calorimeter is parallelepipedic. Therefore, a 3D mesh is required. Due to symmetry, only ¼ of the concrete specimen + calorimeter system is meshed (see Fig. 1). The insulation is provided by the use of a polyurethane foam and air.

2.1.2. Thermal model

The evolution of temperature is obtained from the energy balance equation, which includes the release of heat due to the hydration reaction:

$$c\dot{T} = \nabla(k\nabla T) + L\dot{\xi} \quad (3)$$

in which L is the latent heat of hydration [J m^{-3}], T is the temperature, ξ is the hydration degree, k is the thermal conductivity [W m^{-1} K^{-1}] and c is the volumetric heat capacity [J m^{-3} K^{-1}]. The latent heat of hydration, the thermal conductivity and the volumetric heat capacity are kept constant [24,25]. Considering an evolution of the thermal conductivity and the volumetric heat capacity of concrete (with respect to hydration degree and temperature) leads to a difference of only few degrees [26]. Also, convection and radiation in the air inside the calorimeter (between the concrete specimen and the polyurethane, see Fig. 1) are taken into account by modifying the value of its thermal conductivity (cf. Table 2, Section 3.1.2 and [27]).

The hydration of cement paste is a thermo-activated process, which can be taken into account through an Arrhenius type law (e.g. [17]). Its evolution is modeled by the following relation [14,23]):

$$\dot{\xi} = \widetilde{A}(\xi)\exp\left(-\frac{E_a}{RT}\right) \quad (4)$$

in which $\widetilde{A}(\xi)$ is the normalized chemical affinity, associated with the micro-diffusion process of water which reacts with unhydrated cement [14].

In Eqs. (4) and (5), latent heat of hydration and normalized chemical affinity are identified from a QAB test (after the use of Eqs. (1) and (2), and the procedure given by Ulm and Coussy [14]) performed at the LCPC on a ordinary concrete (see Table 1 for the mix composition).

The boundary conditions are assumed to be of convective type. The convective heat flux (φ) [W m^{-2}] reads:

$$\varphi = h(T_s - T_{ext})\mathbf{n} \quad (5)$$

where h is the coefficient of exchange [W m^{-2} K^{-1}], T_s is the temperature on the surface [K]; T_{ext} is the ambient temperature [K] and $\mathbf{n}$ is the normal unit vector to the surface (oriented towards the exterior). It should be emphasized that parameter h includes convection and radiation (which is linearized since the low variation of temperature, see Section 3.1.2 and [27]).

Thermal parameters are given in Table 2. Classical values for material parameters (thermal conductivity, heat capacity) have been used, expect for the heat capacity of the insulating material which has been deduced from the calibration of the calorimeter (which gives a global heat capacity equal to 3266 J K^{-1}). The chemical affinity and hydration heat release have been deduced analytically from Eq. (1) using several aforementioned hypothesis.

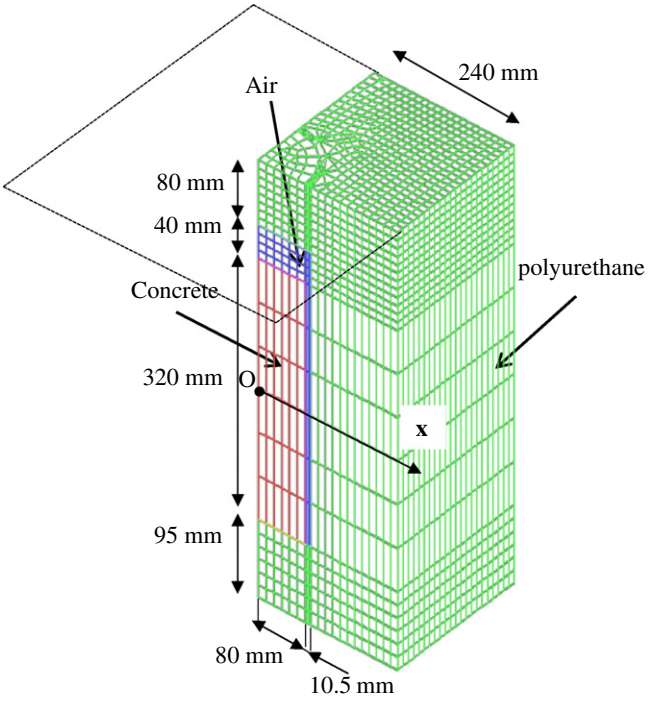

Fig. 1. Mesh of ¼ of the QAB device.

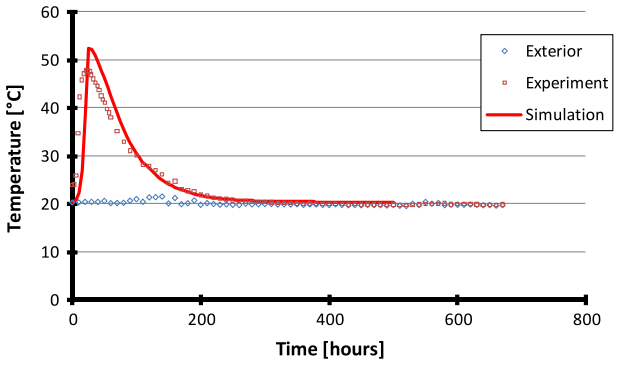

Fig. 2. Evolution of temperature at the center of the concrete specimen (point O in Fig. 1).

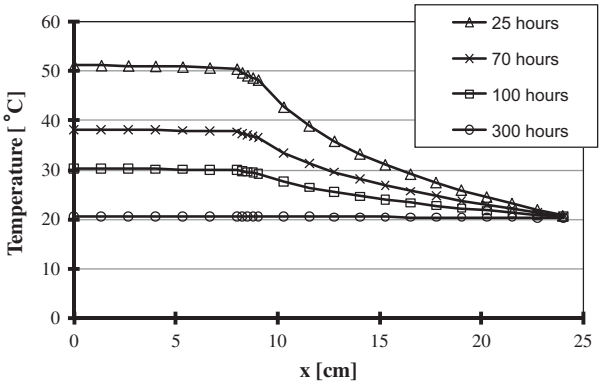

Fig. 3. Evolution of temperature with distance from the center ofthe QAB test specimen (see Fig. 1) at different times.

2.2. Analysis of results

Calculations are performed using subroutines developed by the authors of Cast3m finite element code developed at the Commissariat à l'Energie Atomique [29]. Experimental and predicted evolutions of temperature are plotted in Fig. 2.

A relative good accordance between experimental and numerical results is achieved in terms of kinetics and maximal value. Indeed, the adopted modeling is simplified: the thermal bridges (at the level of the cover and the passage of thermal sensor toward the exterior) and the rigid envelop of the calorimeter, for instance, are not taken into account. Moreover, the precision of the thermal sensors is around a few degrees.

In Fig. 3, the temperature profile with respect to time shows that the temperature is almost homogeneous in the concrete specimen (abscissa less than 0.08 m). It can also be shown on the temperature field at different times displayed in Fig. 4. Therefore, it is not necessary to place precisely the temperature sensor inside the concrete specimen (an accuracy of about 1 or 2 cm is sufficient).

Fig. 5 compares the results in transient (at 25 h) and steady-state conditions (the temperature is imposed uniformly at 51.5 °C and 20.2 °C in the concrete specimen and the exterior, respectively, which corresponds roughly to their values at 25 h in transient conditions). It should be emphasized that the steady-state conditions are reached rapidly (after about 10 h). The two evolutions are almost identical.

Table 1
Mix of concrete.

	Aggregates (kg m^{-3})		Sand (kg m^{-3})	Cement CEM II/A 52.5 (CPJ 55 PM) (kg m^{-3})	Water-reducing plasticizer (L m^{-3})	Water (L m^{-3})
	12.5/25	5/12.5				
OC	783	316	772	350	1.22	201

Table 2
Thermal parameters used in the numerical simulations of the QAB test.

	h (W m^{-2} °C^{-1})	k (W m^{-1} °C^{-1})	C (J m^{-3} °C^{-1})	L (W m^{-3})	E_a/R (K)
Air		0.088[a]	1200		
Insulating		0.03	14,680		
Concrete		1.7	2.4×10^6	140.1×10^6	5500
Down face	0.6 [28]				
Up and lateral faces	9				

[a] Thermal conductivity of air is equal to 0.0257 W m^{-1} °C^{-1} at 20 °C. The (greater) value proposed in this table takes also into account of convective and radiative transfers [27].

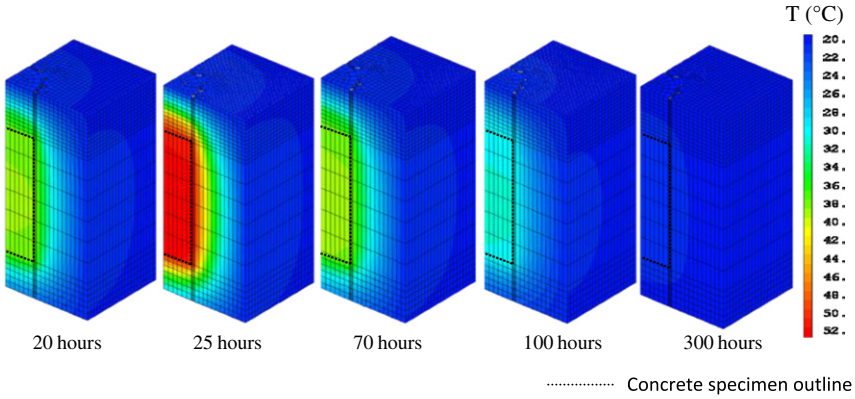

Fig. 4. Temperatures fields at different times during the QAB test.

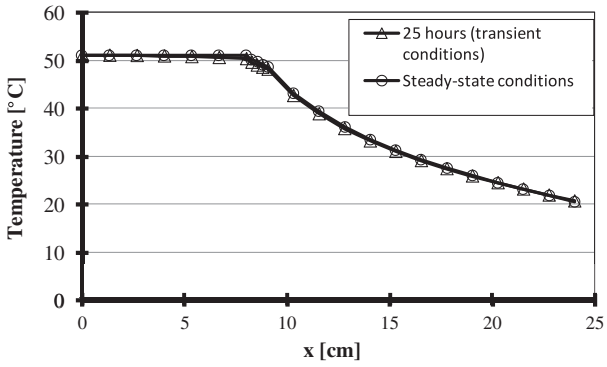

Fig. 5. Spatial evolution of temperature in the QAB test along the **x** axis (see Fig. 1) at 25 h (transient conditions) and steady-state conditions. Temperature of the concrete specimen is imposed uniformly at 51.1 °C.

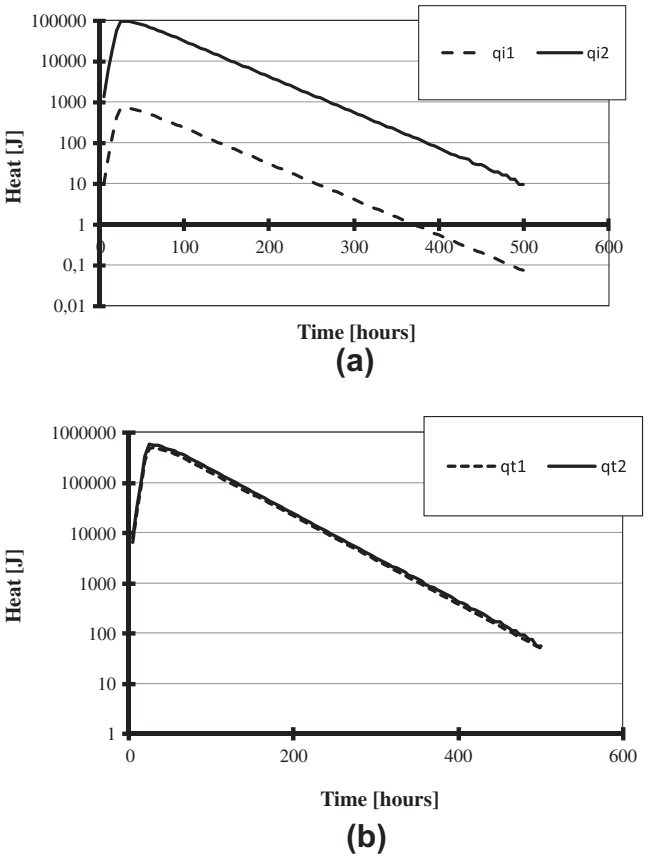

Fig. 6. Evolution of accumulated heat in the insulating q_{i1} (a) and in the whole system (b) (concrete specimen and calorimeter = q_{t1}). Comparison with the value proposed in compensation of heat loss in the QAB test: q_{i2} (a) and q_{t2} (b).

The heat loss compensation, proposed in Eq. (1), supposes that the temperature inside the calorimeter is uniform and equal to the concrete one. However, Figs. 3 and 4 show that this is not the case. In order to evaluate the limit of this assumption, the quantities $q_{i1} = \int_0^t c_{iso}(T_{iso}(t) - T_{iso}(0))dV_{iso}$ which correspond to the real accumulated heat in the insulation (c_{iso} = 14,680 J m^{-3} K^{-1}, cf. Table 2, is the insulating heat capacity) and $q_{i2} = C_{iso}(T_{con}(t) - T_{con}(0))$ which correspond to the accumulated heat in the insulation calculated with the assumption that the temperature inside the calorimeter is uniform and equal to the concrete one (C_{iso} = 3266 J K^{-1} is the total heat capacity of the calorimeter) are compared in Fig. 6a. A huge difference between this quantities is obtained (a ratio of about 135, constant in time), which suggests that Eq. (1) is not valid. It should be noticed that the contribution of air can be neglected (total heat capacity of 3.4 J K^{-1}).

Nevertheless, the total heat capacity of concrete is equal to C_{tot} = 15,440 J K^{-1}, which is about five times greater than the one of the calorimeter (3266 J K^{-1}). Therefore, the quantities $q_{t1} = \int_0^t c_{iso}(T_{iso}(t) - T_{iso}(0))dV_{iso} + c_{con}(T_{con}(t) - T_{con}(0))dV_{con}$ and $q_{t2} = C_{tot}(T_{con}(t) - T_{con}(0))$ which correspond respectively to the real accumulated heat in the whole system and to the accumulated heat in the whole system calculated with the assumption that the temperature inside the calorimeter is uniform and equal to the concrete one are compared in Fig. 6b (which corresponds to the correction proposed in Eq. (1). A weak role of the insulating is shown in the accumulation of heat (but not for the heat loss, since it reduces it through the a and b coefficients). Indeed, the ratio of about 680 is predicted between the accumulation of heat in the concrete and the insulating ($\int_0^t c_{con}(T_{con}(t) - T_{con}(0))dV_{con} \approx 680 \int_0^t c_{iso}(T_{iso}(t) - T_{iso}(0))dV_{iso}$). Therefore, the accumulated heat in the calorimeter can be neglected and Eq. (1) remains valid.

Fig. 7 confirms that a law for the heat loss of the form $y = \alpha(\theta) \cdot \theta$ (with $\alpha(\theta) = a + b\theta$ and b less than a) is valid. Numerical results are close to the experimental ones. Moreover, the coefficient b (which has no real physical meaning) can be neglected (up to heating of $\Delta\theta$ = 40 °C).

Finally, Fig. 8 shows that most of the heat is loss through the lateral sides, as expected (since the lateral surface is greater than the top and bottom ones).

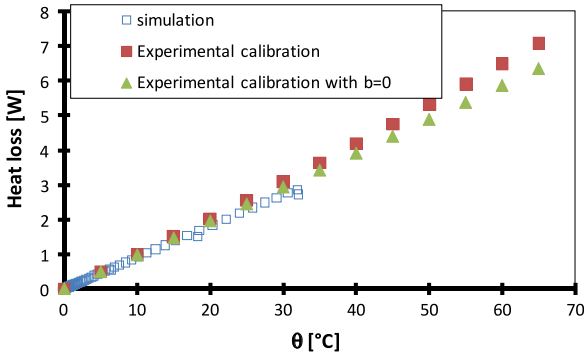

Fig. 7. Evolution of heat loss with respect to heating θ (difference between the concrete specimen and the exterior).

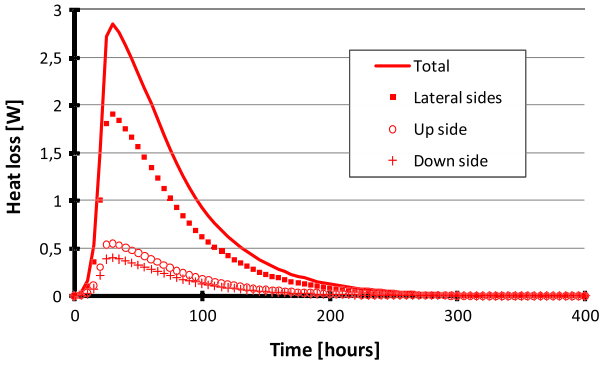

Fig. 8. Evolution of heat loss in the QAB with respect to time through different sides.

3. Langavant test

3.1. Mesh and model

3.1.1. Mesh

Unlike the QAB test, the calorimeter used in the Langavant test and the concrete specimen placed inside it both have a cylindrical shape. This allows axisymmetric numerical simulations to be performed (Fig. 9).

3.1.2. Thermal model

The main difficulty for the Langavant test modeling is to take into account the radiation heat transfer into the vacuum. To simplify the simulations, the heat transfer due to the radiation has been considered as equivalent (non-linear) conduction after linearization of the heat flux. Effectively, the heat flux transmitted between two plates by radiation can be written as following:

$$\varphi = \varepsilon\sigma(T_{int}^4 - T_{ext}^4) \tag{6}$$

where ε is the emissivity of the surface [–], σ is the Stephan–Boltzmann constant [5.67×10^{-8} W m^{-2} K^{-4}], T_{int} is the temperature of the first plate [K] and T_{ext} is the temperature of the second plate [K].

Eq. (6) can be transformed to obtain an equivalent (non-linear) conduction coefficient:

$$\begin{aligned}\varphi &= \varepsilon\sigma(T_{int} - T_{ext})(T_{int}^3 + T_{int}^2 T_{ext} + T_{int} T_{ext}^2 + T_{ext}^3) \\ &\approx 4\varepsilon\sigma T_{moy}^3 (T_{int} - T_{ext}) = \frac{\lambda_{eq}}{e}(T_{int} - T_{ext})\end{aligned} \tag{7}$$

where $T_{moy} = (T_{ext} + T_{int})/2$, e is the tightness of the vacuum room and λ_{eq} [W m^{-1} K^{-1}] is the equivalent thermal conductivity.

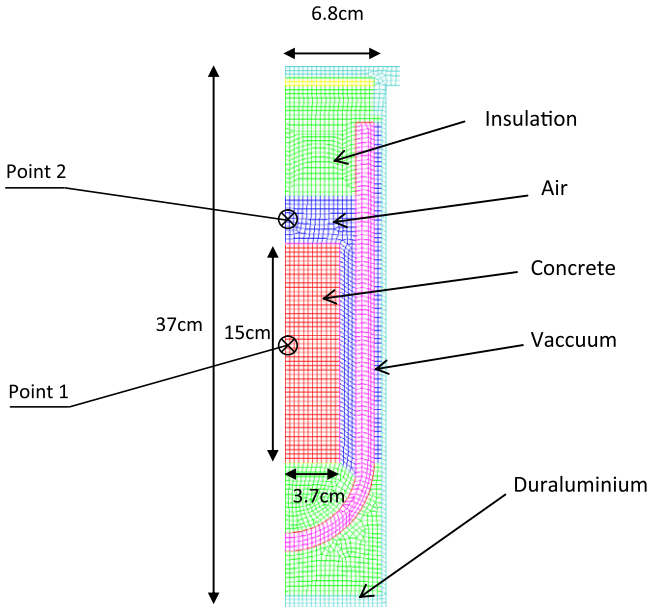

Fig. 9. Axisymetric mesh of the Langavant test.

This approximation which is regularly used (see for example [27]), can only be done if the temperature difference $T_{int} - T_{ext}$ stays in a small interval compared with the radiation heat transfer.

Thus, the Langavant test modeling can be assimilated to a conductive problem. In the virtual mesh of the vacuum room, the conductivity coefficient depends upon the temperature. The model used is the same as presented in Section 2.1.2.

The used thermal parameters are summarized in Table 3.

3.2. Analysis of results

The specimens used in a Langavant test do not have sufficient size to be representative of concrete. Therefore, Schwartzentruber [30] has developed the concept of the equivalent concrete mortar (MBE in French). The principle is to replace the volumetric proportion of aggregates which have a diameter greater than 5 mm by sand by keeping the same specific area with the concrete aggregate one. Designed at first for rheological study, Schwartzentruber [30] has shown that the MBE is also representative of the concrete for calorimetric tests.

Experimental tests and numerical simulations were performed. The evolutions of temperatures are measured or calculated in two distinct locations (the first one is the middle of the specimen of MBE and the second one is the middle of the air located above the specimen; see Fig. 9). These points have been chosen because although the norm recommends placing the temperature sensor in the mortar specimen, it can be interesting to reuse the temperature sensor (by placing it above the specimen). Fig. 10 presents the temperature evolution at two aforementioned points with respect to time.

The results of the comparison are very interesting. Firstly, although the parameter used in the thermo-chemical simulation (chemical affinity) comes from a QAB test, one can observe a good concordance between experimental and numerical results. Thus, the hypothesis of a good representativeness of the MBE with respect to the referenced concrete is validated.

Secondly, one can observe a non-negligible temperature difference between points 1 and 2. This difference invalidates the hypothesis of an almost constant temperature throughout the calorimeter room. This may have important consequences on the total heat release calculation and on the prediction of the hydration

Table 3
Thermal parameters used for the Langavant test simulation.

	ε (–)	h (W m^{-2} °C^{-1})	k (W m^{-1} °C^{-1})	C (J m^{-3} °C^{-1})	L (W m^{-3})	E_a/R (°K^{-1})
Air			0.088	1200		
Insulation			0;043	13,000		
Concrete equivalent mortar			2	2.460×10^6	172.1×10^6	5500
Duraluminium			200	860		
Vacuum room face	0.03					
Free face		9				

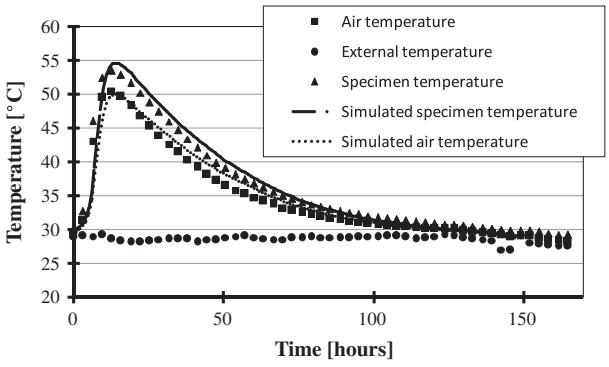

Fig. 10. Temporal evolution of the temperature (points 1 and 2, see Fig. 9) in a Langavant test.

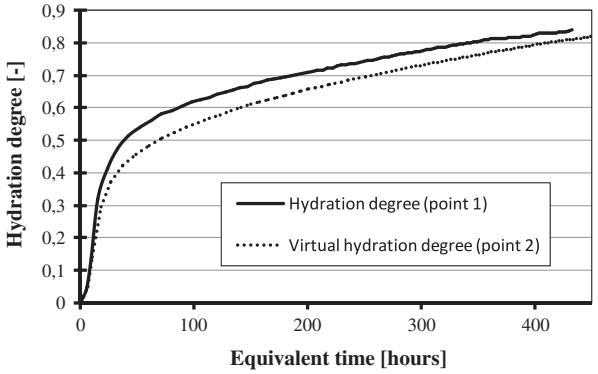

Fig. 12. Hydration degree evolution (from the temperature measurement at points 1 and 2, see Fig. 9).

degree kinetics. Effectively, the hydration degree evolution is calculated from the adiabatic temperature evolution (normalized by the final adiabatic temperature). So, as the temperature evolution kinetics presented in Fig. 10 seems to be approximately the same, it is possible that the hydration degree evolution will not be affected by the temperature difference. Nevertheless, with this approach, the thermo-activation (more important at point 1 than at point 2) is not taken into account. The results of the classical interpretation of Langavant test (through heat losses compensation to obtain the adiabatic temperature and time correction to take into account the thermo-activation) are displayed in Figs. 11 and 12.

Fig. 11 shows an important difference between the two adiabatic temperature evolutions which finally gives an error of 22% on the calculation of the total heat release. For the hydration degree (Fig. 12), the error done is lower but reaches a mean value of 8%.

The comparison of the heat losses obtained by numerical simulation and by the calorimeter calibration is presented in Fig. 13. The heat losses obtained by finite element calculations are slightly lower than the calibration one but a quasi-linear relation is

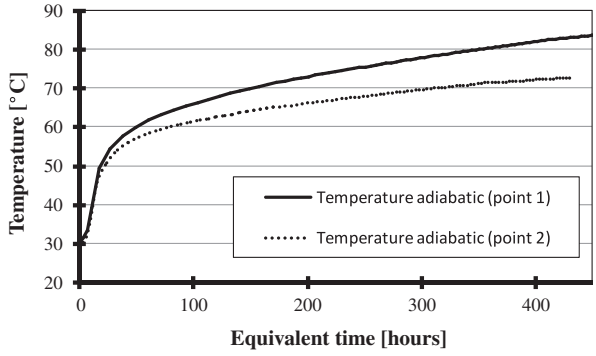

Fig. 11. Calculated adiabatic temperature evolution (from the temperature measurement at points 1 and 2, see Fig. 9).

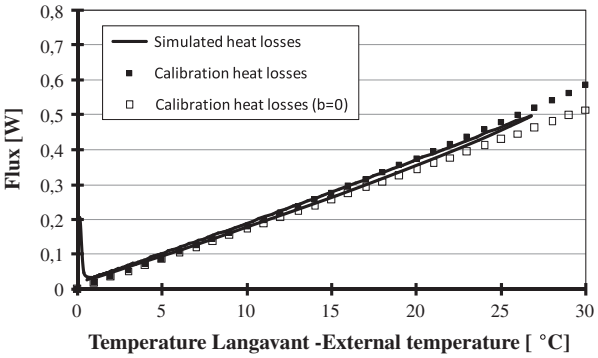

Fig. 13. Heat losses evolution versus the difference between the specimen and external temperatures.

obtained (following the form: $y = \alpha\theta$) with $\alpha = a + b\theta$ like in the QAB test.

4. Influence of apparent activation energy

As we have seen previously, the cement apparent activation energy is needed in the QAB and Langavant tests analysis for the determination of the hydration degree evolution. Moreover, it appears in the calculation of the chemical affinity (equally determined from the calorimetric test results) through the following equation [14]:

$$A(t) = \xi_\infty \frac{dT^{ad}/dt}{T_\infty^{ad} - T_0^{ad}} exp\left(\frac{E_a}{RT(t)}\right) \quad (8)$$

where ξ_∞ is the final hydration degree [–] (which could be obtained with the empirical law proposed by Waller [24]).

Thus, in a numerical simulation, this parameter appears two times (one time explicitly in the calculation of the hydration degree, Eq. (5), and a second time implicitly in the calculation of the chemical affinity, Eq. (8). A parametrical study based on the apparent activation energy has been performed to highlight the

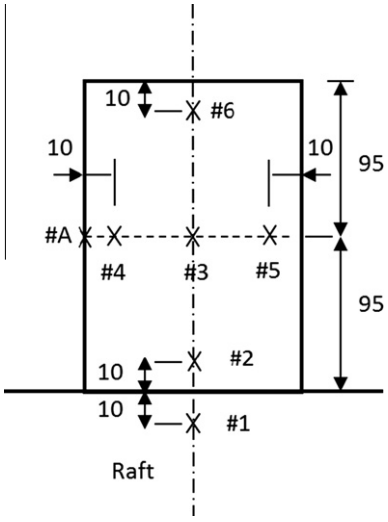

Fig. 14. Wall dimensions and temperature sensor positions (distance in cm).

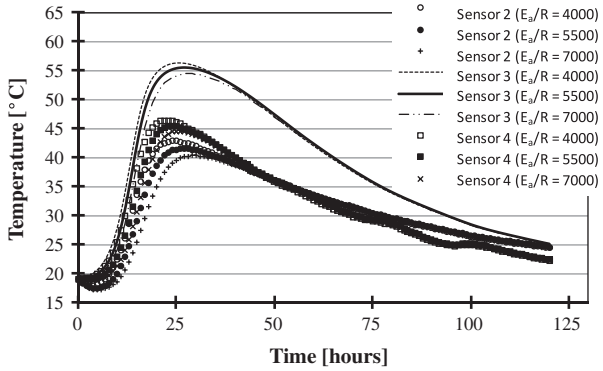

Fig. 15. Evolution of the predicted temperature inside the wall at different locations (see Fig. 14) for different activation energies.

effect of this parameter on the calculation of temperature evolution in a massive structure. A simple geometry, representative of a massive wall cast on a massive slab, has been considered and the temperature fields during the hydration have been calculated. The wall dimensions and the position of the temperature sensor are displayed in Fig. 14. The evolution of the adiabatic temperature used comes from a QAB test.

A constant value of the apparent activation energy has been used for each simulation (see the introduction). The simulations performed covers a large scale of apparent activation energy values (from $E_a/R = 4000\ K^{-1}$ to $E_a/R = 7000\ K^{-1}$). Fig. 15 shows the parametrical study results. In the simulation, the chemical affinity is recalculated for each value of apparent activation energy.

The simulations results highlight a weak effect of the apparent activation energy on the maximal temperature reached for each temperature sensors but also on the temperature evolution kinetics. This can be explained by the fact that the chemical affinity calculated from a semi-adiabatic (or adiabatic) test plays a compensatory role of the energy activation value. So, it is necessary to consider the couple $(A(\xi), E_a/R)$.

Furthermore, this study shows that an approximate value of the apparent activation energy (calculated for example from the cement chemistry given by Kishi and Maekawa [31] quoted in Buffo-Laccarrière [32] or Schindler [18]) is sufficient to predict correctly the temperature field evolution of a massive structure. Thus, only one calorimetric test (semi-adiabatic or adiabatic) is necessary if the chemical affinity is calculated with this apparent activation energy.

5. Conclusion

Simulations of (semi-adiabatic) calorimetric tests like QAB and Langavant test allow us to validate some hypotheses made for the interpretation (through heat loss compensation) and to invalidate some simplifications of the test protocol (and quantification of the mistakes):

- Even though the calorimeters calibration is performed under steady-state conditions, whereas the test is performed under transient conditions, the heat losses can be calculated by the following equation $y = \alpha\theta$, with $\alpha = a + b\theta$.
- In the QAB test, the accumulated heat in the insulation can be neglected. Therefore, the analytical equation (Eq. (1)) proposed which includes the accumulated heat and the heat losses are validated by numerical simulations.
- Even though the use of a size of calorimeter compatible with the aggregate size of the tested material is always preferred, the used of an equivalent concrete mortar and a Langavant calorimeter can be sufficient to obtain the total heat release and the chemical affinity of the concrete.
- A wrong position of the temperature sensor (outside the specimen) in a Langavant test leads to an important error on the total heat release calculation and to a non-negligible error on the hydration degree evolution. Nevertheless, an accuracy of about 1 or 2 cm on the temperature sensor position inside the specimen is largely sufficient.

Finally, a parametrical study of the apparent activation energy effect has shown the possibility to use an approximate value of it, provided that the couple $(A(\xi), E_a/R)$ is considered. The experimental determination of an accurate value needs to perform two semi-adiabatic tests in two different environments (two external temperatures for example). This requires adequate equipment and increases the cost of conducting the experiments. The results of this study seem to show that only one semi-adiabatic test is sufficient to predict correctly the temperature field evolution inside a massive concrete structure.

References

[1] Branco FA, Mendes PA, Mirambell E. Heat of hydration effects in concrete structures. ACI Mater J 1992;89(2):139–45.
[2] Pinto RCA, Hover KC. Superplacticizer and silica fume addiction effects on heat hydration of mortar mixtures with low water–cementitious materials ratio. ACI Mater J 1999;96(5):600–5.
[3] Bai J, Wild S. Investigation of the temperature change and heat evolution of mortar incorporating PFA and metakaolin. Cem Concr Compos 2002;24(2):201–9.
[4] Ng PL, Ng IYT, Kwan AKH. Heat loss compensation in semi-adiabatic curing test of concrete. ACI Mater J 2008;105(1):52–61.
[5] Suzuki Y, Harad S, Maekawa K, Tsuji Y. Evaluation of adiabatic temperature rise of concrete measured with the new testing apparatus. Proc Jpn Soc Civ Eng 1988;396(9):109–18.
[6] Coole MJ. Heat release characteristics of concrete containing ground granulated blastfurnace slag in simulated large pours. Mag Concr Res 1988;40(144):152–8.
[7] Bamforth PB. In-situ measurement of the effect of partial Portland cement replacement using either fly ash or ground granulated blast-furnace slag on the early age behaviour of mass concrete. Taylor Woodrow research project no. 014J/77/1939; 1977.
[8] Costa U. A simplified model of adiabatic calorimeter. Il Cem 1979;76(2):75–92.
[9] Springenschmidt R. Prevention of thermal cracking in concrete at early ages–state of the art report. London: E&FN Spon; 1998.
[10] NF P 15-436. Mesure de la chaleur d'hydratation des ciments par calorimétrie semiadiabatique dite méthode du calorimètre de Langavant, AFNOR; 1988 [in French].
[11] NF EN 196-9. Méthode d'essais des ciments. Partie 9: Chaleur d'hydratation Méthode semi-adiabatique. AFNOR; 2004 [in French].

[12] Acker P. Thermal effect in concrete during manufacture and applications to engineering structures. Ann Inst Tech Bâtiment Travaux Publ 1986;442:61–80.
[13] Cesar LCPC. Finite element code, Module TEXO, LCPC software v3.2; 1994 [in French].
[14] Ulm F-J, Coussy O. Couplings in early-age concrete: from material modelling to structural design. Int J Solids Struct 1998;35(31–32):4295–311.
[15] Waller V, d'Aloïa L, Cussigh F, Lecrux S. Using the maturity method in concrete cracking control at early ages. Cem Concr Compos 2004;26:589–99.
[16] Benboudjema F, Torrenti JM. Early age behaviour of concrete nuclear containments. Nucl Eng Des 2008;10(238):2495–506.
[17] Regourd M, Gauthier E. Comportement des ciments soumis à un durcissement accéléré. Ann l'ITBTP 1980;179:65–96 [in French].
[18] Schindler AK. Effect of temperature on hydration of cementitious materials. ACI Mater J 2004;101(1):72–81.
[19] D'Aloïa L, Chanvillard G. Determining the "apparent" activation energy of concrete Ea—numerical simulations of the heat of hydration of cement. Cem Concr Res 2002;32(8):1277–89.
[20] Broda M, Wirquin E, Duthoit B. Conception of an isothermal calorimeter for concrete – determination of the apparent activation energy. Mater Struct 2002;35:389–94.
[21] Ballim Y, Graham PC. Early age heat evolution of clinker cements in relation to microstructure and composition: implications for temperature development in large concrete elements. Cem Concr Compos 2004;26(5):417–26.
[22] Xiong X, Van Breugel K. Isothermal calorimetry study of blended cements and its application in numerical simulations. Heron 2001;46(3):151–9.
[23] Lackner R, Mang HA. Chemoplastic material model for the simulation of early-age cracking: from the constitutive law to numerical analyses of massive concrete structures. Cem Concr Compos 2004;26:551–62.
[24] Waller V. Relations entre composition des bétons, exothermie en cours de prise et résistance en compression. PhD thesis, Marne-La-Vallée, Ecole Nationale des Ponts et Chaussées; 2000 [in French].
[25] Mounanga P. Étude expérimentale du comportement de pâtes de ciment au très jeune âge: hydratation, retraits, propriétés thermophysiques. PhD thesis, Nantes, Université de Nantes; 2004.
[26] Briffaut M, Benboudjema F, Torrenti JM, Nahas G. Effects of the early age thermal behavior on the long term damage risks of massive structures. Eur J Environ Civ Eng. submitted for publication.
[27] Hernot H, Porcher G. Thermique appliquée aux bâtiments. Paris: Editions parisiennes; 1984. ISBN2862430153 [in French].
[28] Clement JL. Comportement du béton au jeune âge. In: Paul Acker, Jean-Michel Torrenti, Franz-Josef Ulm, Mim Traité, editors. série Matériaux de construction; 2004 [in French].
[29] Commissariat à l'Energie Atomique CEA – DEN/DM2S/SEMT, Code éléments finis Cast3m, disponible sur <http://www-cast3m.cea.fr/>.
[30] Schwartzentruber A. Catherine C La méthode du mortier de béton équivalent (MBE). Un nouvel outil d'aide à la formulation des bétons adjuvantés. Mater Struct 2000;33:475–82 [in French].
[31] Kishi T, Maekawa K. Thermal and mechanical modelling of young concrete based on hydration process of multi-component cement materials. In: Rilem proceeding thermal cracking in concrete at early age; 1994. p. 11–9. ISBN 0-419-18710-3.
[32] Buffo Lacarrière L. Prévision et évaluation de la fissuration précoce des ouvrages en béton. PhD thesis, Toulouse, Thèse de l'université de Toulouse; 2007 [in French].